International Journal of Heat and Mass Transfer 111 (2017) 484–494

Contents lists available at ScienceDirect

International Journal of Heat and Mass Transfer

journal homepage: www.elsevier.com/locate/ijhmt

Single phase laminar flow and heat transfer characteristics of microgaps with longitudinal vortex generator array

Jian-Fei Zhang [a], Yogendra K. Joshi [b,*], Wen-Quan Tao [a]

[a] Key Laboratory of Thermo-Fluid Science and Engineering of MOE, School of Energy and Power Engineering, Xi'an Jiaotong University, Xi'an 710049, China
[b] George W. Woodruff School of Mechanical Engineering, Georgia Institute of Technology, Atlanta, GA 30332-0405, United States

ARTICLE INFO

Article history:
Received 15 January 2017
Received in revised form 12 March 2017
Accepted 12 March 2017
Available online 12 April 2017

ABSTRACT

We study the integration of longitudinal vortex generators (LVGs) into microgaps for heat transfer augmentation via three-dimensional steady numerical simulations Firstly, the impacts of geometric parameters, including transverse spacing of LVG pairs, height of microgaps, and number of LVG pairs in the flow direction were considered. Then the heat transfer and flow resistance of LVG enhanced micro-gap were compared with smooth micro-gap. The results show that the flow resistance and heat transfer performance of LVGs enhanced microgaps decrease with increase in transverse spacing of LVGs. Microgaps with larger heights do not demonstrate a significant increase in heat transfer performance, but have much lower pressure drop. The microgap equipped with more LVG pairs has higher pressure drop and heat transfer coefficients. Finally, compared with the smooth microgap, the overall enhancement ratio of all studied LVGs enhanced microgaps increases with *Re*, and the overall enhancement ratios of specific LVGs enhanced microgap model is larger than one over the full range of *Re* being studied. The present study is intended to promote the development of new heat transfer enhancement technique in microgaps.

1. Introduction

With continued reduction in semiconductor feature size, power dissipation has become a limiting factor for higher-performance integrated circuits [1–4]. Three-dimensional (3D) stacked electronics present multiple advantages, including shorter interconnect lengths and the possibility of heterogeneous integration, such as logic and memory in a single device. However, the challenging thermal problem of significantly increased heat flux per chip footprint area must be overcome before 3D stacked electronics can be adopted for practical applications. To address the challenges in cooling of 3D stacked electronics, inter-tier microfluidic cooling, applying micro pin fin array in the microgap between tiers of 3D stack, has recently been employed. Such pin fin enhanced microgaps have been recently studied, including single-phase forced microfluidic cooling [5–9], two-phase microfluidic cooling [10–15], and configuration optimization of pin fins [16,17]. Besides the application in 3D ICs cooling, Li et al. studied micro-scale cooling for turbine blade surfaces by using pin-fin arrays [18,19].

Here we investigate LVGs as heat transfer enhancement features within microgaps. Jacobi and Shah [20], and Fiebig [21] have classified the flow disturbances used for heat transfer enhancement, in general, into transverse vortex generators (TVGs) and longitudinal vortex generators (LVGs). As pointed out by them, various pin-fin shapes can be classified as TVGs, which mainly generate transverse vortices-having their axes perpendicular to the flow direction. However, LVGs can generate longitudinal vortices with their axes in the flow direction. The longitudinal vortices persist for long distances in the flow direction, diffusing very slowly, thus exhibiting a promising potential for heat transfer enhancement. Since the 1990', the LVG has been introduced into large-scale heat transfer equipment, as a so called fourth generation heat transfer enhancement technique [22–29]. Some researchers also used LVGs to enhance the heat transfer in thermoelectric generator systems [30–32]. Recently, researchers have started to apply LVGs for enhancing the heat transfer in microchannels.

Liu et al. [33] carried out experiments on the flow and heat transfer in rectangular microchannels with and without LVGs. It was found that the LVGs can enhance the heat transfer in microchannel at the expense of a larger pressure drop. They also found that the laminar to turbulent transition is affected by the number, and the attack angle of LVGs. Empirical correlations for apparent friction factor and Nusselt number were developed. Extending the work of Liu et al. [33], Chen et al. [34] investigated the heat transfer in microchannels with different hydraulic diameters, and different heights of LVGs. They demonstrated that the overall heat transfer performance of some specific

* Corresponding author.
E-mail address: yogendra.joshi@me.gatech.edu (Y.K. Joshi).

http://dx.doi.org/10.1016/j.ijheatmasstransfer.2017.03.036
0017-9310/

Nomenclature

Latin symbols

A	area, m^2
A_c	cross sectional area of the inlet, m^2
A_{chip}	area of chip, m^2
A_p	projected area of the heated chip, m^2
b	width of the LVG, m
c_p	specific heat, $kJ/(kg \cdot K)$
D_h	hydraulic diameter, m
f	fanning friction factor
H_1	thickness of the chip, m
H_2	height of the microgap, m
h	heat transfer coefficient based on project area, $W \cdot (m^2 \cdot K)^{-1}$
h_{wet}	heat transfer coefficient based on the total wetted area, $W \cdot (m^2 \cdot K)^{-1}$
k	thermal conductivity, $W \cdot (m \cdot K)^{-1}$
L_1	length of the chip, m
L_2	stream-wise spacing of LVG pairs, m
l	length of the LVG, m
Nu	Nusselt number
Δp	pressure drop, Pa
p	static pressure, Pa
Q	total power applied on the heating surface, W
R	thermal resistance, K/W
Re	Reynolds number
ΔT	temperature differences, K
T	temperature, K
U_{in}	inlet velocity, $m \cdot s^{-1}$
u	velocity, $m \cdot s^{-1}$;
W_1	width of the chip, m
W_2	spacing between two LVG in transvers direction, m
W_3	spacing between two LVG pairs in transvers direction, m

Greek symbols

β	attack angle of LVG
η_{total}	overall fin efficiency of LVG array
μ	dynamic viscosity, Pa·s
ρ	density, $kg \cdot m^{-3}$

Subscripts

avg	average
cond	conduction
conv	convection
f	fluid
s	surface
smooth	smooth microgap

microchannels with LVGs was better than the corresponding smooth microchannel.

Ebrahimi et al. [35] conducted numerical analysis on the heat transfer of single phase laminar flow in rectangular microchannels equipped with two pairs of LVGs. They considered the influence of attack angle of the LVGs on the heat transfer performance. The results showed that the *Nu* and the friction factor for microchannels with LVGs were increased by 2–25% and 4–30% respectively. Ebrahimi et al. [36] also numerically studied the heat transfer for nanofluids (water-Al_2O_3 and water-CuO) in a rectangular microchannel with six pairs of LVGs. It was found that heat transfer could be enhanced greatly, compared to pure water. By using the same geometric model as in [36], Sabaghan et al. [37] performed numerical simulations of the flow and heat transfer of TiO_2-based nanofluids, and found heat transfer augmentation by using LVGs.

To the author's knowledge, there are only limited studies on the heat transfer enhancement in microchannels using LVGs. In these studies, only few LVGs (up to six pairs) were used in a single microchannel, with no studies focusing on microgaps ($H_2/W_1 \ll 1$ compared with microchannel, where H_2 is the height and W_1 the width of the flow passage). Also, a constant-temperature boundary condition was adopted by most of the microchannel studies [33–35]. A constant wall heat flux boundary condition is more in line with many electronic cooling applications. As another heat transfer surface modification approach, Wei et al. [38] applied dimples on the surface of micro-channels, which also showed heat transfer augmentation. However, the dimple array configuration does not allow electrical connectivity between the tiers of 3D stacked chips. Therefore, in this paper, we propose incorporatings LVGs into microgaps, and investigate the impact of LVGs arrays (up to around one thousand LVGs) on the heat transfer enhancement within microgaps with a constant wall heat flux boundary condition. We numerically study the single phase laminar flow and heat transfer, and discuss the impact of different geometric parameters on the heat transfer performance. The heat transfer performance of LVGs enhanced microgaps is compared with that of smooth microgap.

2. Geometric configurations and parameters

Fig. 1 indicates the arrangement of LVG array, and the definition of dimensions of the heated chip and LVGs. The size of the chip is 1 cm × 1 cm, the length of the LVG, l, is 200 μm, the width of the LVG, b, is 50 μm, and the attack angle (β) of the LVG is 45°. The thickness of the chip, H_1, is 100 μm in this study. More details about the geometric parameters of the different configurations are shown in Table 1.

3. Computational model and numerical method

Figs. 2 and 3 demonstrate the computational domain and boundary conditions. There is no gap between the tip of LVG and the top wall of the microgap. The inlet block is used to represent the flow development zone and the outlet block is used to prevent reverse flow at the outlet surface. Symmetric boundary conditions are applied between the LVGs to reduce the computational domain and computational cost. A uniform heat flux, 100 W/cm^2, is applied under the chip. Non-slip boundary condition is applied on all solid surfaces within the computational domain. Heat conduction within LVGs and the chip is considered by using coupled heat transfer module in ANSYS FLUENT [39].

The material of LVGs and chip is Si. Deionized-water (DI-water) is used as the coolant with the inlet temperature being 25 °C. The temperature-dependent thermo-physical properties for Si and DI-water are adopted in the calculation (Table 2) [35]. The deionized-water flow is assumed to be incompressible. The range of inlet velocity is determined based on the critical Reynolds number suggested by Liu et al. [33], to make sure all the computations are in the laminar region.

3.1. Numerical method

ANSYS FLUENT 15.0 is used to calculate the flow and heat transfer in the computational model. The QUICK scheme is used to

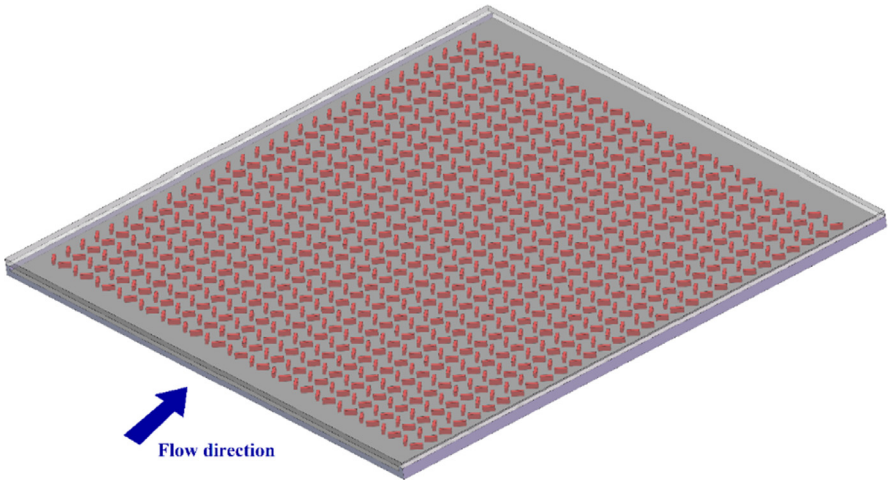

(a) LVGs array incorporated in a heated microgap (top cover is shown as transparent)

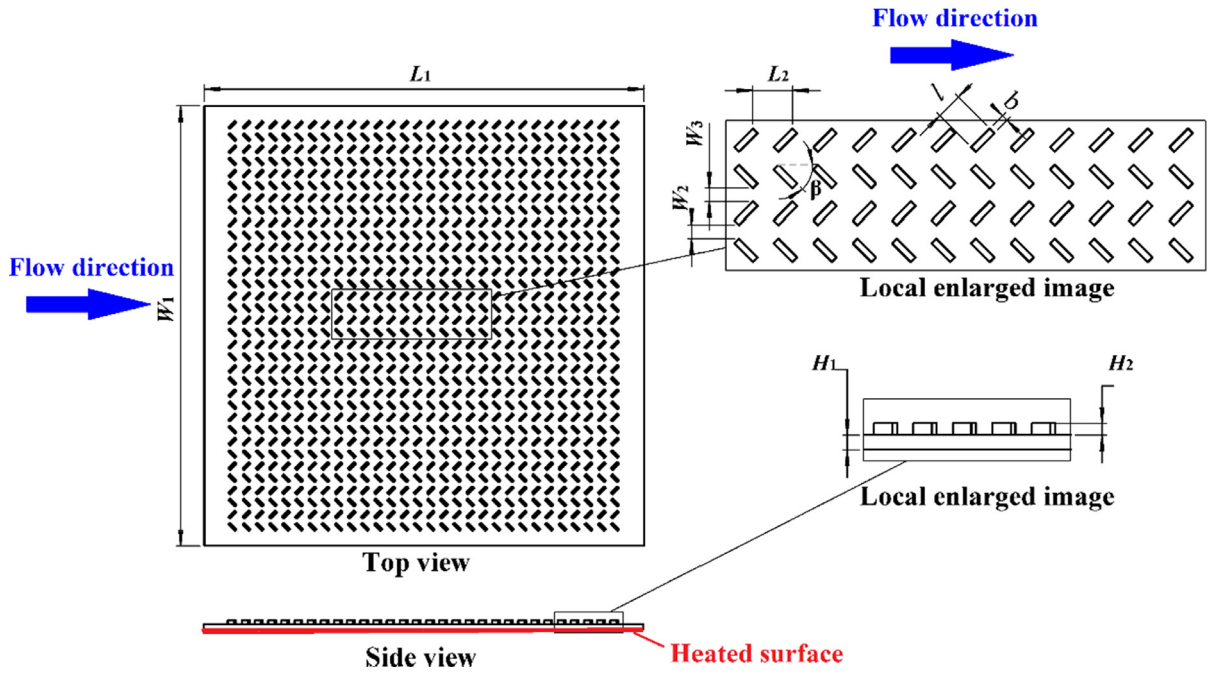

(b) Geometric parameters

Fig. 1. Arrangement of LVG array and geometric parameters.

Table 1
Geometrical parameters for different configurations (unit: μm).

Model No.	Number of LVG in flow direction	L_2	W_2	W_3	H_2	l	b
1	30	300	100	100	100	200	50
2	30	300	100	150	100	200	50
3	30	300	100	200	100	200	50
4	30	300	100	100	125	200	50
5	30	300	100	100	150	200	50
6	40	250	100	100	100	200	50

discretize the convective terms. The SIMPLE algorithm is adopted to deal with the coupling between velocity and pressure. Despite the convergence criterion for mass residual (less than 10^{-6}), momentum residual (less than 10^{-6}) and energy residual (less than 10^{-8}), the average inlet and outlet pressure of the DI-water, the average temperature of the bottom wall of the chip, and the average outlet temperature of the DI-water are also monitored during the calculation for convergence judgment.

3.2. Grid independence test

The computational domain is discretized with the sweep method to generate structural mesh, and the regions adjacent to the LVGs, and top and bottom solid surface of the microgap are meshed much finer (see Fig. 4). A grid independence study are carried out before undertaking the calculations. Seven different grid systems are used in the grid independence test of model 1 and the results of the heat transfer coefficient and pressure drop at highest inlet velocities are presented in Table 3. The results show that the differences of pressure drop and *Nu* between the fifth and seventh grid systems are both less than 1%. So, the fifth grid system is chosen as a balance between the computational cost,

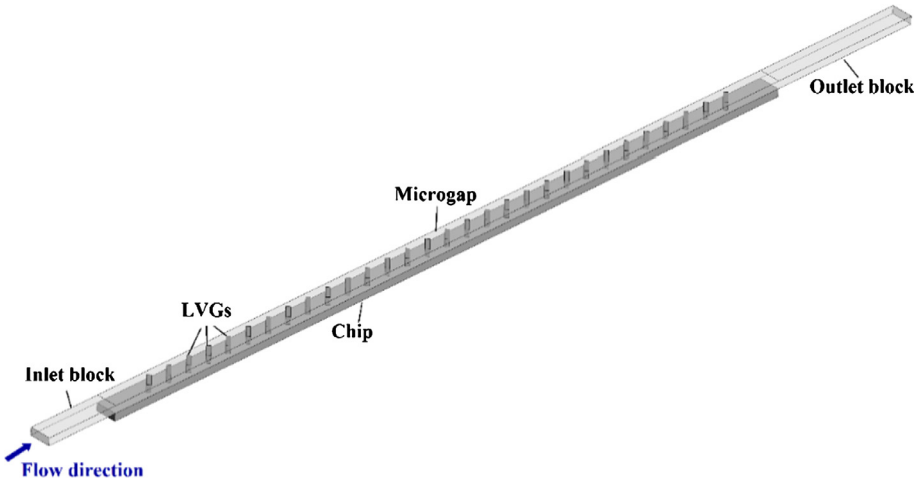

Fig. 2. Computational model.

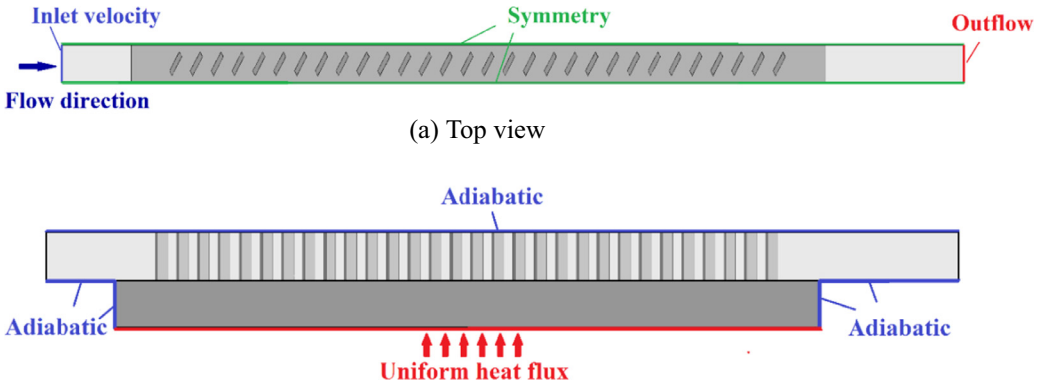

Fig. 3. Boundary conditions (not drawn to scale).

Table 2
Temperature-dependent thermo-physical properties of DI-water and Si [35].

Properties	Silicon	Deionized-water
μ (Pa·s)	/	$0.0194–1.065\times10^{-4}T+1.489\times10^{-7}T^2$
k (W/(m·K))	$290–0.4T$	$-0.829+0.0079T-1.04\times10^{-5}T^2$
c_p (J/(kg·K))	$390+0.9T$	$5348–7.42T+1.17\times10^{-2}T^2$
ρ (kg/m^3)	2330	998.2

and solution accuracy. Table 4 shows the mesh number for all of the computational models.

3.3. Numerical method validation

In order to verify the accuracy and reliability of the numerical method in the present study, a validation model is built based on the "microchannel G2" in the experimental study of Liu et al. [33]. Figs. 5 and 6 compare the experimental data and numerical results for friction factor and average *Nu* respectively. The differences are around 0.05–5% for *Nu* and 25–32% for friction factor. It should be noted that in the study of Liu et al. the pressure drop being used to calculate the friction factor was derived by subtracting the pressure drop at the bends, entrance, and exit from the measured overall pressure drop. Uncertainties in empirical coefficients and correlations adopted to predict the pressure drops at the bends, entrance, and exit were not addressed. Also, the experimental uncertainties in determining the friction factor and *Nu* for microchannel G2 are reported as 5.7% and 16.9%, respectively. Based on the above factors, the agreement between the numerical and experimental results is considered acceptable.

4. Results and discussions

The *Re* is defined as follows.

$$Re=\frac{\rho U_{\mathrm{in}}D_{\mathrm{h}}}{\mu} \tag{1}$$

where

$$D_{\mathrm{h}}=\frac{4A_{\mathrm{c}}}{P_{\mathrm{w}}}=\frac{2W_1H_2}{W_1+H_2} \tag{2}$$

where A_c is cross sectional area of the inlet, P_w is wetted perimeter of the microgap, U_{in} is the inlet velocity. The Nusselt number can be calculated by the following relation.

$$Nu=\frac{hD_{\mathrm{h}}}{k} \tag{3}$$

The thermal resistance between the heating surface and the fluid is defined as [8]

$$R=\frac{\Delta T}{Q}=\frac{T_{s,avg}-T_{f,avg}}{Q} \tag{4}$$

where Q is the total power applied to the heating surface, $T_{s,avg}$ is the average temperature of the heated surface, $T_{f,avg}$ is the average

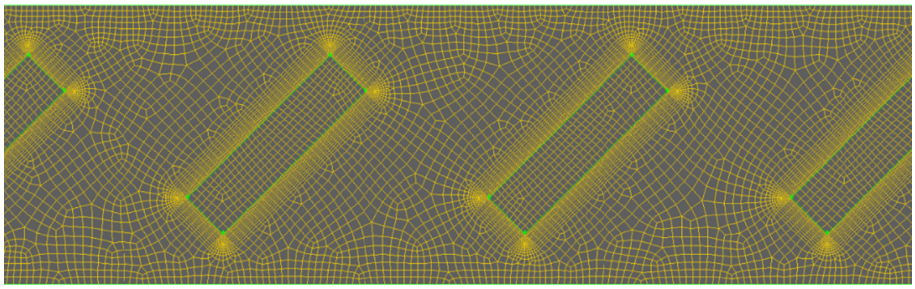

(a) Meshes around the LVGs

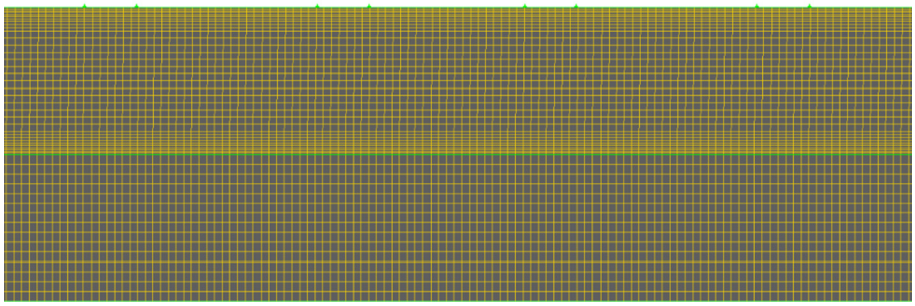

(b) Meshes on the side face of channel and chip

Fig. 4. Meshes of computational model.

Table 3
Grid independent test for Model 1.

Mesh number	Inlet velocity: 1.2 m/s			
	Δp/Pa	Differences/%	h/(W·m^{-2}·K^{-1})	Differences/%
753,891	62263.18	−8.01	49097.15	−8.39%
2,086,380	67212.50	−16.59	55384.64	−22.27%
3,163,308	60735.79	−5.36	49244.99	−8.72%
4,004,274	56887.63	1.32	44947.54	0.77%
4,745,160	57279.40	0.64	45154.60	0.31%
6,007,350	57719.88	−0.12	45540.26	−0.54%
6,784,750	57647.90	0	45296.31	0

Table 4
Mesh number used in numerical calculation.

Model No.	1	2	3	4	5	6
Mesh number	4,745,160	4,679,540	4,984,109	5,165,208	5,654,771	5,529,993

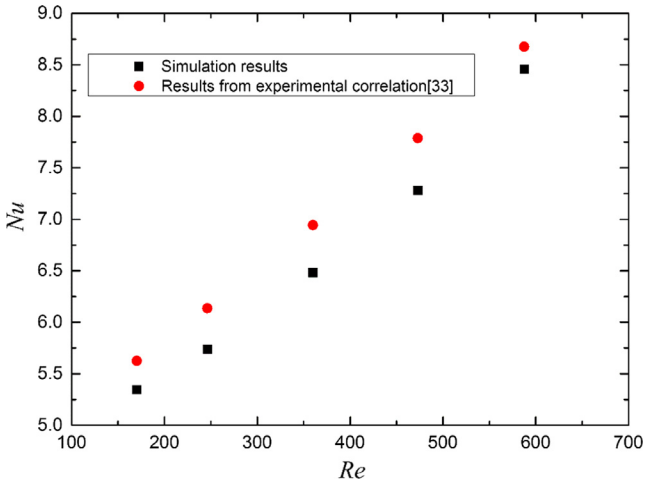

Fig. 5. Validation of *Nu* with experimental results of Liu et al. [33].

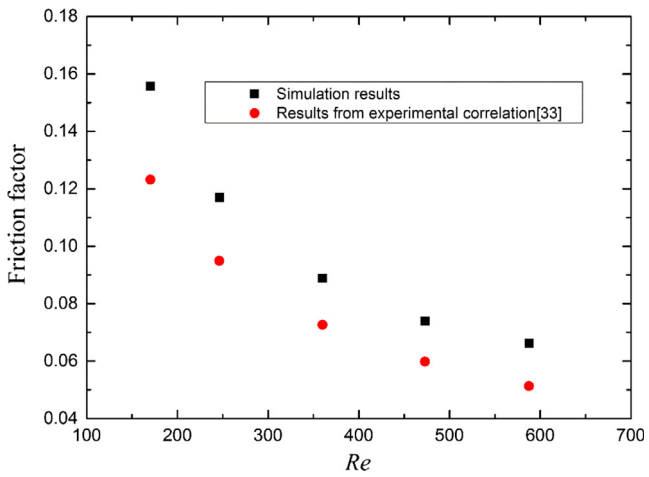

Fig. 6. Validation of friction factor with experimental results of Liu et al. [33].

fluid temperature. Here R includes the conduction resistance across the chip, and the convection resistance between the solid and fluid.

$$R = R_{cond} + R_{conv} \tag{5}$$

$$R_{cond} = \frac{H_1}{k_{chip} A_{chip}} \tag{6}$$

where k_{chip} is the thermal conductivity of the chip, A_{chip} the area of chip, and H_1 is the thickness of chip.

$$R_{conv} = \frac{1}{hA_p} \tag{7}$$

$$h = h_{wet}\eta_{total} \tag{8}$$

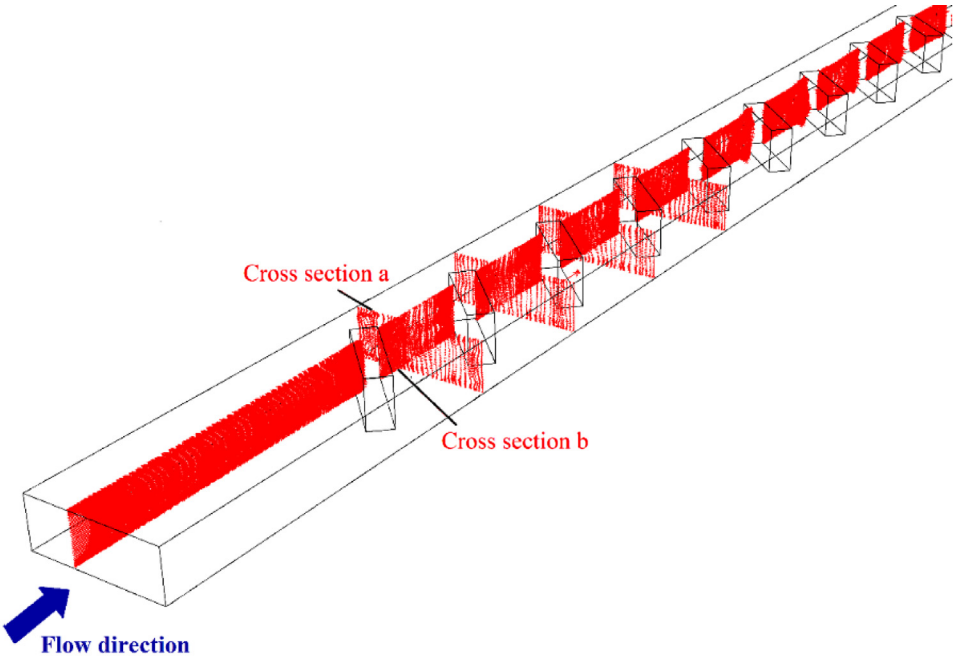

(a) Locations of cross sections

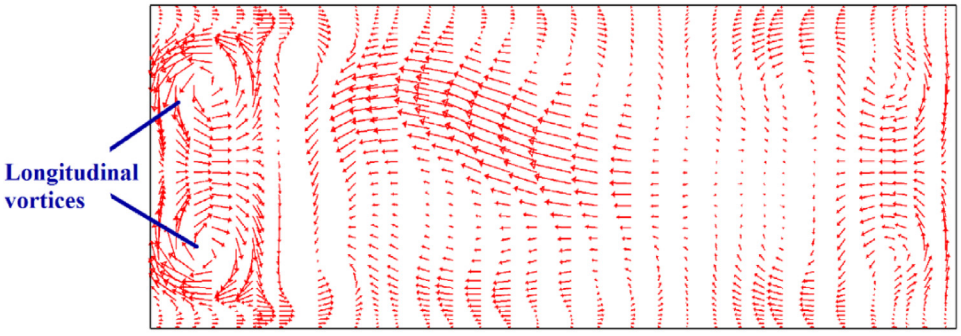

(b) Cross section a

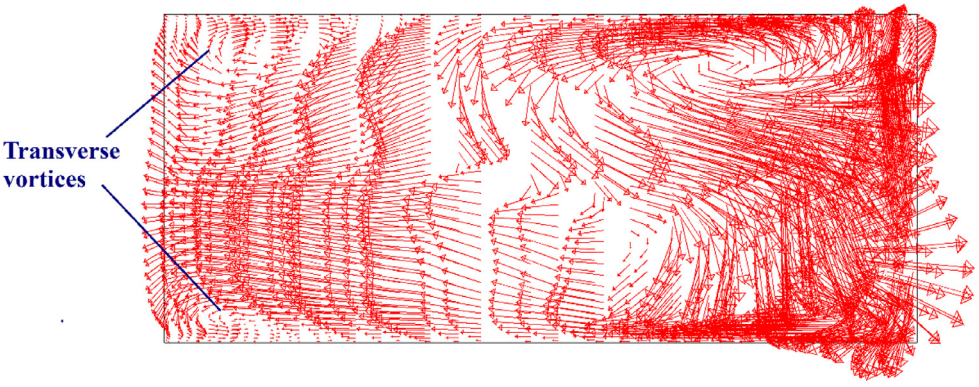

(c) Cross section b

Fig. 7. Velocity distributions in specified cross sections.

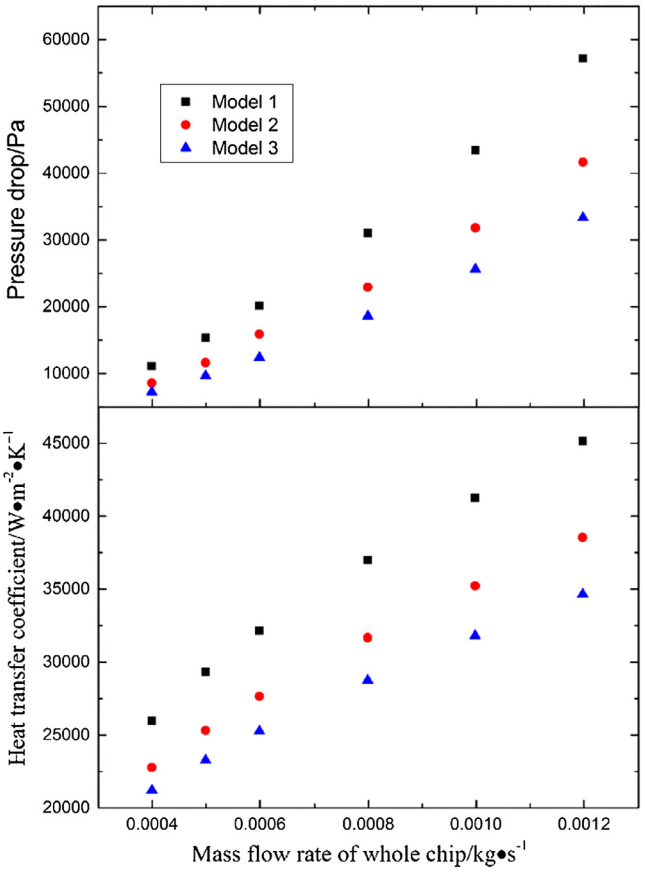

Fig. 8. Pressure drop and heat transfer coefficient for Model 1, Model 2, and Model 3.

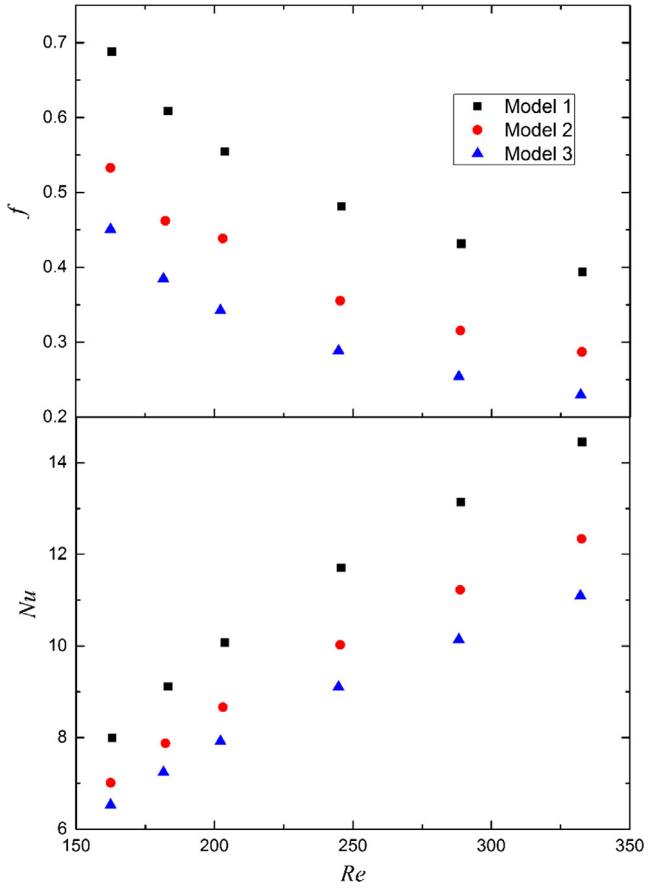

Fig. 9. Friction factor and *Nu* for Model 1, Model 2, and Model 3.

where A_p is the projected area of the heated chip with LVGs arrays ($A_p = L_1 \times W_1$), h_{wet} is heat transfer coefficient based on the total wetted area of LVGs enhanced chip, and η_{total} is the overall fin efficiency of LVGs array. The heat transfer coefficient h is defined base on the projected area A_p, so it involves the overall fin surface efficiency of LVG enhanced surface, and reflects the overall heat transfer enhancement performance of the enhanced surface.

The fanning friction factor is defined as follows [8]:

$$f = \frac{D_h \Delta p}{2L_1 \rho U_{in}^2} \tag{9}$$

4.1. Effects of transverse spacing (W_3) of LVG pairs (Models 1, 2 and 3)

Fig. 7 shows the velocity distribution in specified local cross-sections. Cross-section a is perpendicular to flow direction. Cross-section b is parallel to the flow direction, and lies between two adjacent LVGs in the flow direction. The features of longitudinal vortices can be clearly observed from the velocity distribution in top left and top right corner of Fig. 7(b). Transverse vortices can also be found in Fig. 7(c). These vortices not only lead to destabilization of the streamwise flow and initiation of boundary layer disturbances, but are also responsible for the increased pressure drop.

Figs. 8 and 9 demonstrate the influences of transverse spacing (W_3) on pressure drop, heat transfer coefficient, friction factor, and *Nu*. It can be seen that the flow resistance and heat transfer performance decrease with the increase of W_3, since the local variation of velocities in the transversal space of adjacent LVG decreases, and the interaction of vortices generated by adjacent LVG pairs in transversal direction also decreases. However, it should be noted that the degree of decrease in the flow resistance and heat transfer performance falls down with increase of W_3.

Fig. 10 shows temperature distribution of fluid in the middle plane of microgap height direction for Model1, Model 2 and Model 3 at same flow rate. Fig. 11 shows temperature distribution in top wall of the chip for Model 1, Model 2 and Model 3 at same flow rate. It is noticeable that the working fluid in Model 1 has more uniform temperature distribution and the chip in Model 1 has lower temperature level than Model 2 and Model 3, which verifies that the heat transfer capacity of Model 1 is the best.

4.2. Effects of the height (H_2) of micogap (Models 1, 4, and 5)

Fig. 12 shows that the model with larger height has lower pressure drop. This is because the velocity in the microgap decreases greatly with the increase of H_2 at fixed mass flow rate, and the end wall effect also becomes smaller. It can also be observed from Fig. 12 that the microgaps having larger height do not demonstrate a much better heat transfer performance compared with those having lower height. This is because all LVGs have the same height as the microgap, so that the microgap having larger height possess larger heat transfer surface area, which has a positive effect on the heat transfer capability. However, at fixed flow rate, the velocity in the microgap with lager height is smaller, which deteriorates the heat transfer. So that Model 4 and 5 does not show a significant increases in the heat transfer coefficients compared with Model 1. Since a larger height of microgap leads to a larger hydraulic diameter and a lower velocity at fixed mass flow rate, according to Eqs. (3) and (9), the *Nu* and friction factor both show increase along with increasing microgap height in Fig. 13.

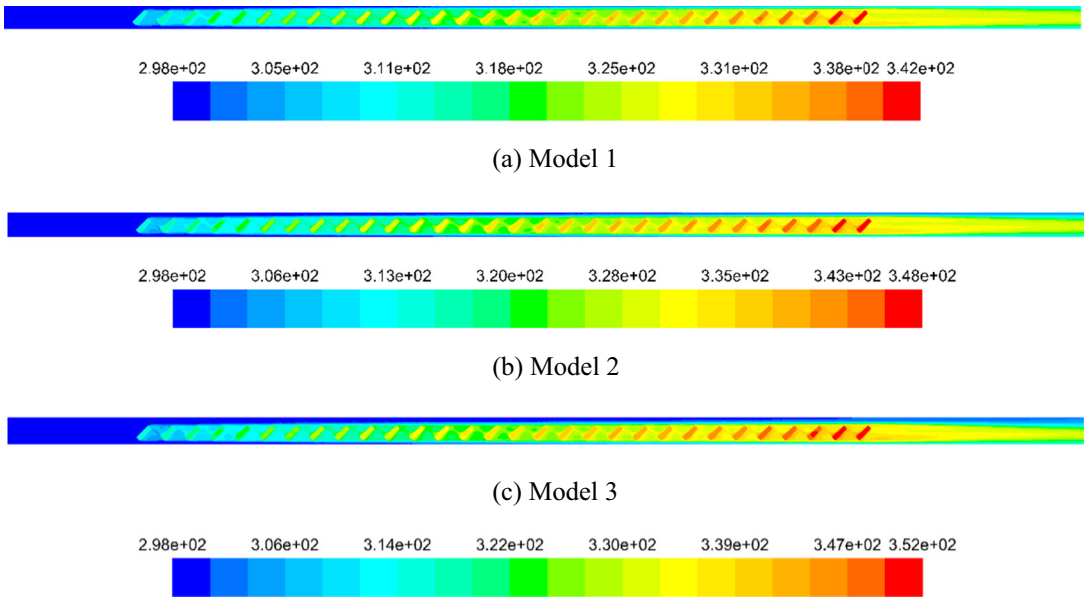

Fig. 10. Temperature distribution in the middle plane of microgap height direction for Model 1, Model 2 and Model 3.

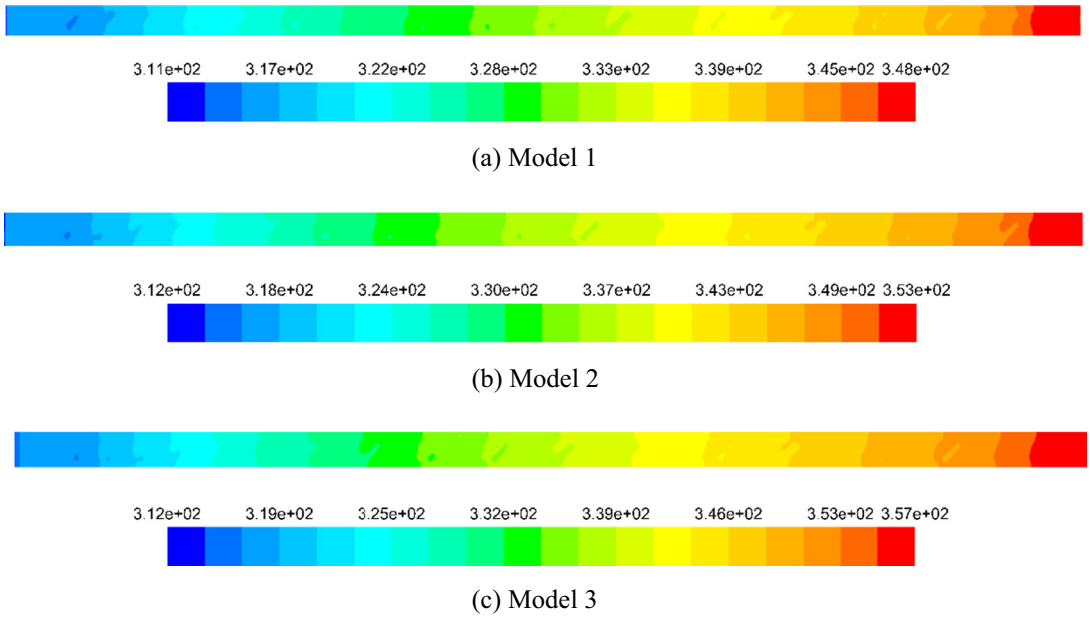

Fig. 11. Temperature distribution in the top wall of chip for Model1, Model 2 and Model 3.

4.3. Effects of the number of LVG pairs (Model 1 and 6)

The flow and heat transfer performance among microgaps with different number of LVG pairs in the flow direction can be observed from Figs. 14 and 15. It can be concluded that Model 6 has higher flow resistance and better heat transfer performance because it has more pairs of LVGs than Model 1, which causes larger heat exchange areas and stronger flow disturbances, thus enhancing heat transfer capability in microgap.

4.4. Overall heat transfer performance analysis

In order to evaluate the overall heat transfer performance of LVGs enhanced microgap, we also calculated the pressure drop and heat transfer characteristics of a smooth microgap with the same length, width, and height as Model 1. Fig. 16 provides the summary of flow resistance and heat transfer performance for all the simulation models. It can be seen that the pressure drop, and heat transfer coefficient of LVGs enhanced microgaps are higher than that of the smooth microgap. This is due to the flow disturbances and complex vortex interactions induced by LVGs. Model 5 has lager height of LVGs, and Model 6 has more LVGs, resulting in lager heat transfer surface area for both, which leads to a higher heat transfer coefficient among all of the Models. However, since the increased heat transfer surfaces of Model 6 are mainly located downstream of the main flow, these surfaces contribute more to the pressure drop penalty than the heat transfer enhancement. The increased heat transfer surface area of Model 5 is distributed

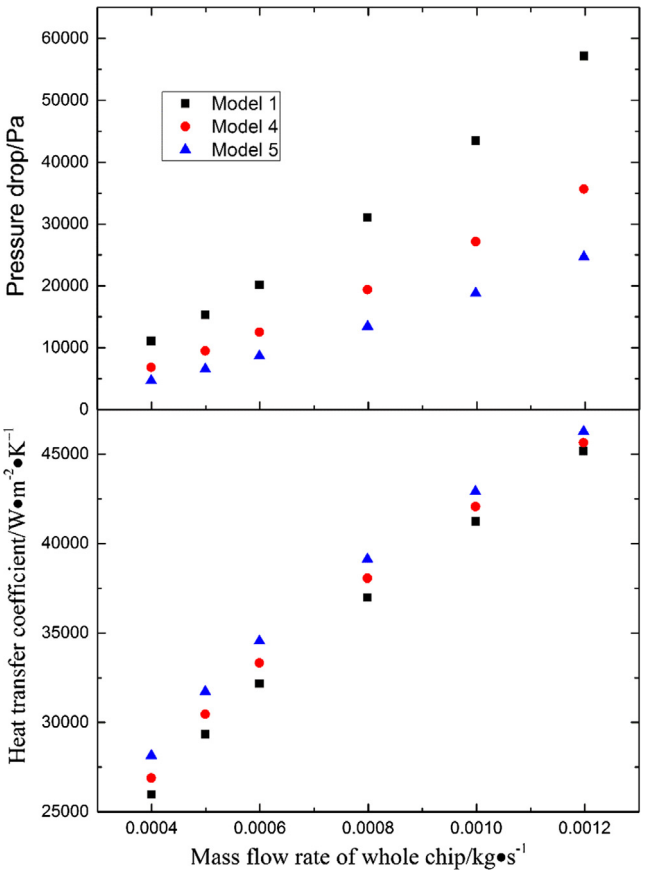

Fig. 12. Pressure drop and heat transfer coefficient for Model 1, Model 4, and Model 5.

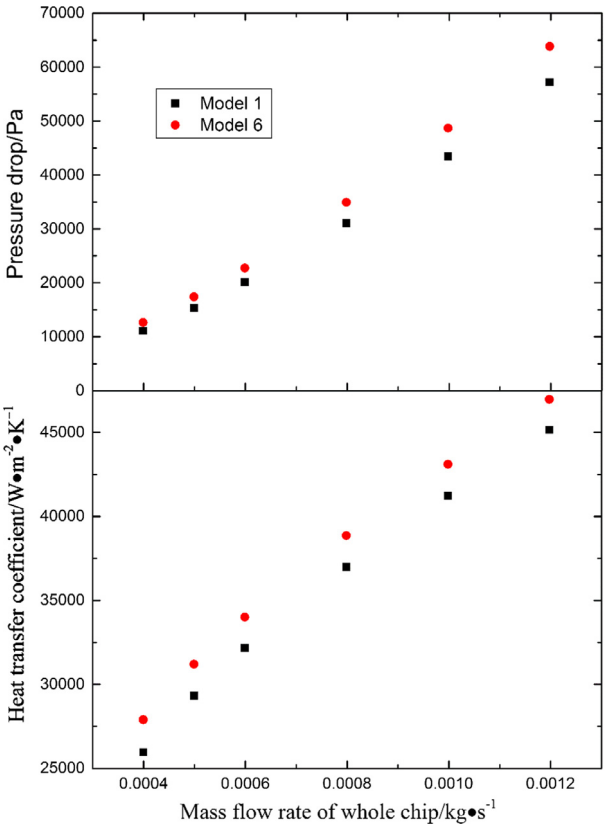

Fig. 14. Pressure drop and heat transfer coefficient for Model 1 and Model 6.

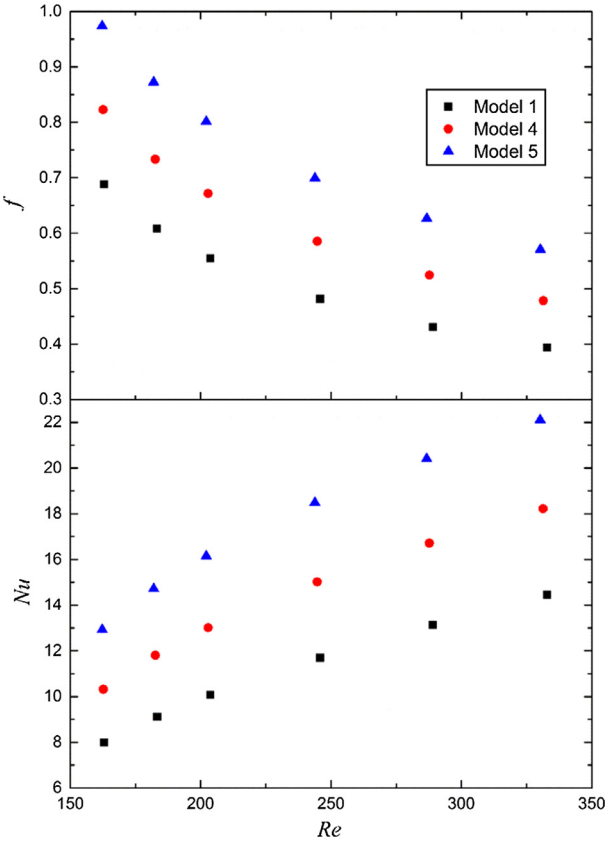

Fig. 13. Friction factor and *Nu* for Model 1, Model 4, and Model 5.

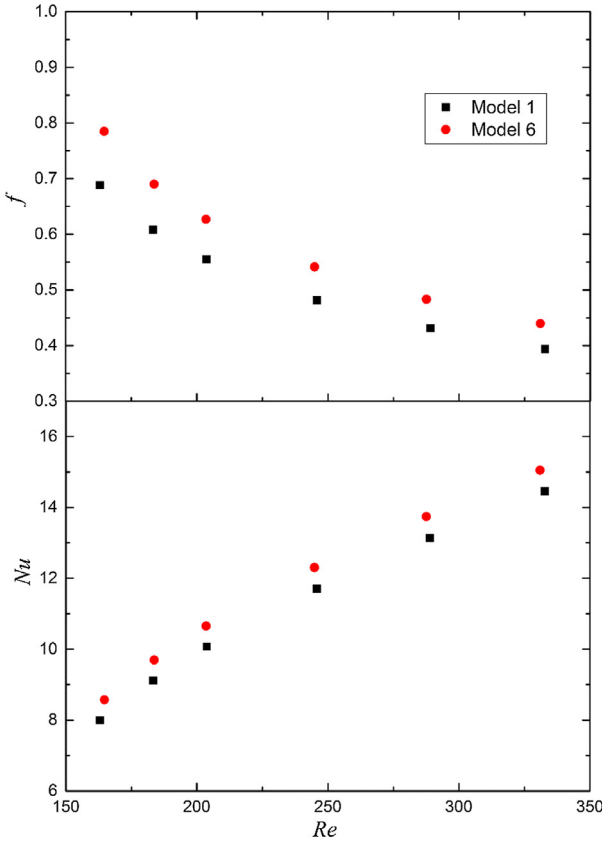

Fig. 15. Friction factor and *Nu* for Model 1and Model 6.

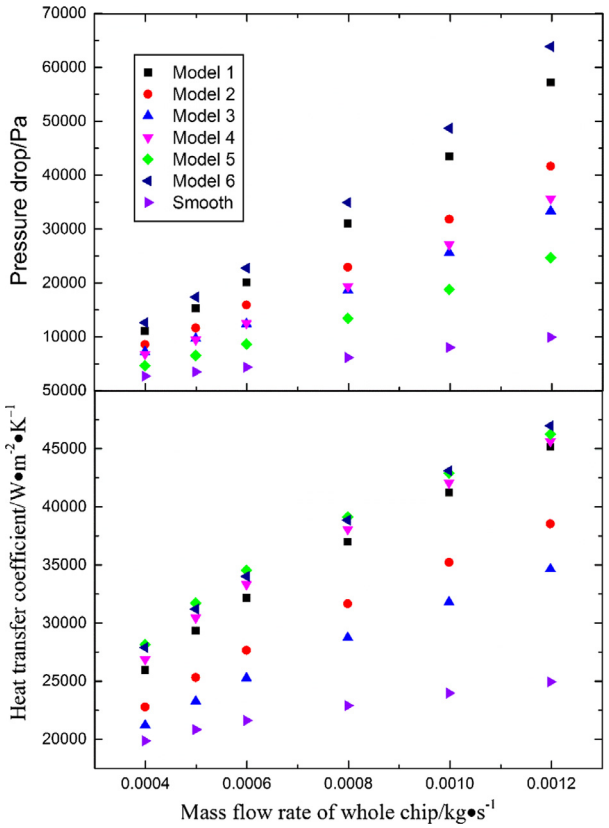

Fig. 16. Pressure drop and heat transfer coefficient of all simulation models.

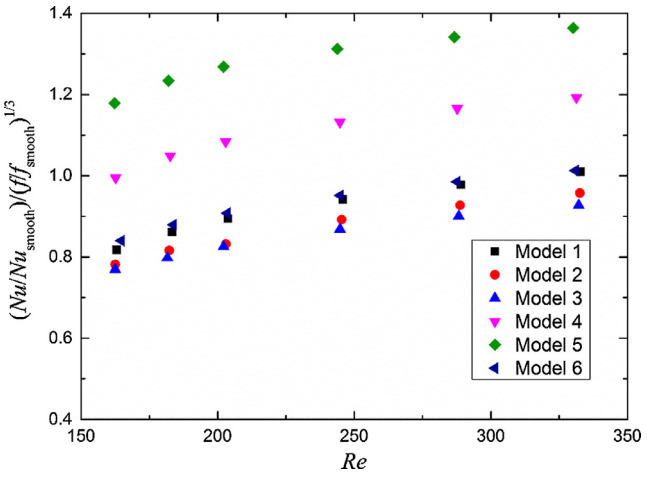

Fig. 17. Overall efficiency of LVGs enhanced microgaps.

evenly through the flow passage, which impacts the heat transfer enhancement more than the flow resistance, so that Model 5 has comparable heat transfer coefficient and lower pressure drop compared with Model 6.

Fig. 17 shows overall enhancement ratio of LVG enhanced microgaps, defined as $(Nu/Nu_{smooth})/(f/f_{smooth})^{1/3}$, where subscript "smooth" represents smooth microgap. This overall enhancement ratio considers both the heat transfer augmentation and the flow resistance increase, and is frequently used to evaluate the overall performance of the heat transfer devices [35,36,40,41]. It can be seen that the overall enhancement ratio is much higher at larger Reynolds number, which means that the longitudinal vortices become much stronger and intensify the fluid mixing and disturbance. Because Model 5 has better heat transfer performance and lower flow resistance, it also shows the best overall heat transfer performance, and its overall enhancement ratios are 1.17–1.36 within the full range of *Re* studied.

Fig. 18 compares the temperature distribution on the top wall of the chip of Model 5, and smooth microgap at the same flow rate. It can be clearly observed that Model 5 results in lower chip temperature levels.

5. Conclusion

In the present study, we investigate longitudinal vortices to intensify heat transfer in a microgap. Three dimensional simulations are performed for the single phase laminar flow and heat transfer characteristics of LVGs enhanced microgap. Different geometrical configurations are considered, and overall enhancement ratios for LVGs enhanced microgaps are compared with a smooth microgap. The conclusions reached are as follows:

1. The existence of longitudinal vortices can induce flow disturbances and disrupt the boundary layer, thus exhibiting a promising augmentation of heat transfer compared with the smooth microgap. Simultaneously, the blockage of LVGs, and the interactions between the vortices induced by LVGs leads to an increase in the pressure drop penalty.
2. The transverse spacing, number of LVG pairs, and the height of the microgaps play important role in the flow and heat transfer characteristics of LVGs enhanced microgaps. The heat transfer performance improves with decrease in transverse spacing, and increase in height of microgaps and number of LVG pairs.

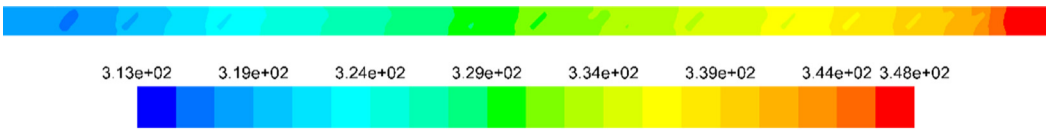

(a) Model 5

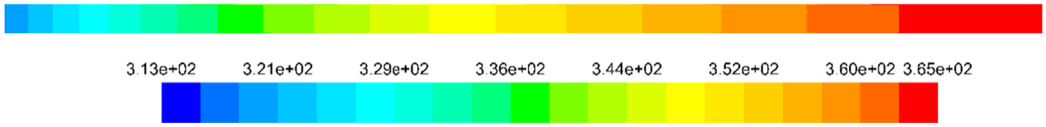

(b) Smooth channel

Fig. 18. Temperature distributions on top wall of chip for Model 5, and smooth microgap.

3. The overall enhancement ratio increases with the *Re*, and could be larger than one for specific microgaps over the full range of *Re* studied.

Acknowledgments

This work is supported by the National Natural Science Foundation of China (NO. 51576155) and China Scholarship Council. The first author acknowledges the support of Georgia Institute of Technology in hosting him as a visiting scholar during 2016.

References

[1] S. Kuhn, M. Kleiner, P. Ramm, W. Weber, Interconnect capacitances, crosstalk and signal delay in vertically integrated circuits, Int. Electron Devices Meet. (1995) 249–252.
[2] T. Brunschwiler, B. Michel, H. Rothuizen, U. Kloter, B. Wunderle, H. Oppermann, and H. Reichl, Foced convective interlayer cooling in vertically integrated packages, in: Proceedings of Intersociety Conference on Thermal and Thermomechanical Phenomena in Electronic Systems, 2008, pp. 1114–1125.
[3] Y. Zhang, A. Dembla, Y. Joshi, M. Bakir, 3D stacked microouidic cooling for high-performance 3D ICs, in: Proceedings of Electronic Components and Technology Conference, 2011, pp. 1644–1650.
[4] S.G. Kandlikar, Review and projections of integrated cooling systems for three-dimensional integrated circuits, J. Electron. Packag. 136 (2014) 024001.
[5] W.L. Qu, A. Siu-Ho, Liquid single-phase flow in an array of micro-pin-fins—Part I: Heat transfer characteristics, J. Heat Transfer 130 (2008) 122402.
[6] W.L. Qu, A. Siu-Ho, Liquid single-phase flow in an array of micro-pin-fins—Part II: Pressure drop characteristics, J. Heat Transfer 130 (2008) 124501.
[7] C.A. Konishi, R. Hwu, W. L Qu, F. E., Pfefferkorn, Experimental study and numerical analysis of water single-phase pressure drop across a micro-pin-fin array, Proceedings of the 14th International Heat Transfer Conference, 2010, IHTC14-23171.
[8] Z.M. Wan, Y. Joshi, Pressure drop and heat transfer characteristics of pin fin enhanced microgaps in single phase microfluidic cooling, in: Proceedings of the ASME 2013 International Mechanical Engineering Congress and Exposition, 2013, IMECE2013-65618.
[9] A. Fabio, G. Sacha, K.T. Manish, T. Brunschwiler, B. Michel, D. Poulikakos, Computational modeling of hot-spot identification and control in 3-d stacked chips with integrated cooling, Numer. Heat Transfer, Part A 65 (2014) 201–215.
[10] S. Krishnamurthy, Y. Peles, Flow boiling of water in a circular staggered micro-pin fin heat sink, Int. J. Heat Mass Transfer 51 (2008) 1349–1364.
[11] W.L. Qu, A. Siu-Ho, Measurement and prediction of pressure drop in a two-phase micro-pin-fin heat sink, Int. J. Heat Mass Transfer 52 (2009) 5173–5184.
[12] Y.J. Kim, Y. Joshi, A.G. Fedorov, Y.J. Lee, S.K. Lim, Thermal characterization of interlayer microfluidic cooling of three-dimensional integrated circuits with nonuniform heat flux, J. Heat Transfer 132 (2010) 041009.
[13] S.A. Isaacs, Y. Joshi, Y. Zhang, M.S. Bakir, Y.J. Kim, Two-phase flow and heat transfer in pin-fin enhanced micro-gaps with non-uniform heating, in: S. Saran (Ed.), Proceedings of the ASME 2013 4th International Conference on Micro/Nanoscale Heat and Mass Transfer, 2013.
[14] A. Reeser, A. Bar-Cohen, G. Hetsroni, High quality flow boiling heat transfer and pressure drop in microgap pin fin arrays, Int. J. Heat Mass Transfer 78 (2014) 974–985.
[15] Y. Madhour, B.P. d'Entremont, J.B. Marcinichen, B. Michel, J.R. Thome, Modeling of two-phase evaporative heat transfer in three-dimensional multicavity high performance microprocessor chip stacks, J. Electron. Packag. 136 (2014) 021006.
[16] S.R. Reddy, G.S. Dulikravich, Multi-objective optimization of micro pin-fin arrays for cooling of high heat flux electronics, in: Proceedings of the ASME 2015 International Mechanical Engineering Congress & Exposition, 2015, IMECE2015-54166.
[17] A. Abdoli, G. Jimenez, G.S. Dulikravich, Thermo-fluid analysis of micro pin-fin array cooling configurations for high heat fluxes with a hot spot, Int. J. Thermal Sci. 90 (2015) 290–297.
[18] W.H. Li, J. Ren, H.D., Jiang, Y.G. Luan, P. Ligrani, Assessment of six turbulence models for modeling and predicting narrow passage flows, Part 2: Pin fin arrays, Numer. Heat Transfer, Part A 69 (5) (2016) 445–463.
[19] P.M. Ligrani, Heat transfer augmentation technologies for internal cooling of turbine components of gas turbine engines, Int. J. Rotat. Mach. 2013 (2013).
[20] A.M. Jacobi, R.K. Shah, Heat transfer surface enhancement through the use of longitudinal vortices: a review of recent progress, Exp. Thermal Fluid Sci. 11 (1995) 295–309.
[21] M. Fiebig, Vortices, generators and heat transfer, Trans. Instit. Chem. Eng. 76 (1998) 108–123.
[22] J.M. Wu, W.Q. Tao, Numerical study on laminar convection heat transfer in a rectangular channel with longitudinal vortex generator. Part A: Verification of field synergy principle, Int. J. Heat Mass Transfer 51 (5–6) (2008) 1179–1191.
[23] J.M. Wu, W.Q. Tao, Numerical study on laminar convection heat transfer in a channel with longitudinal vortex generator. Part B: Parametric study of major influence factors, Int. J. Heat Mass Transfer 51 (13–14) (2008) 3683–3692.
[24] A. Lemouedda, M. Breuer, E. Franz, T. Botsch, A. Delgado, Optimization of the angle of attack of delta-winglet vortex generators in a plate-fin-and-tube heat exchanger, Int. J. Heat Mass Transfer 53 (23–24) (2010) 5386–5399.
[25] M. Zeng, L.H. Tang, M. Lin, Q.W. Wang, Optimization of heat exchangers with vortex-generator fin by Taguchi method, Appl. Thermal Eng. 30 (13) (2010) 1775–1783.
[26] Y.L. He, Y.W. Zhang, Advances and outlooks of heat transfer enhancement by longitudinal vortex generators, Advan. Heat Transfer 44 (2012) 119–185.
[27] H.E. Ahmeda, H.A. Mohammedb, M.Z. Yusoff, An overview on heat transfer augmentation using vortex generators and nanofluids: approaches and applications, Renew. Sustain. Energy Rev. 16 (2015) 5951–5993.
[28] M.J. Li, W.J. Zhou, J.F. Zhang, J.F. Fan, Y.L. He, W.Q. Tao, Heat transfer and pressure performance of a plain fin with radiantly arranged winglets around each tube in fin-and-tube heat transfer surface, Int. J. Heat Mass Transfer 70 (2014) 734–744.
[29] L.O. Salviano, D.J. Dezan, J.I. Yanagihara, Optimization of winglet-type vortex generator positions and angles in plate-fin compact heat exchanger: response surface methodology and direct optimization, Int. J. Heat Mass Transfer 82 (2015) 373–387.
[30] T. Ma, J. Pandit, S.V. Ekkad, S.T. Huxtable, S. Deshpande, Q.W. Wang, Study on thermoelectric-hydraulic performance of longitudinal vortex generators in a large-scale thermoelectric power generator, Energy Proc. 75 (2015) 639–644.
[31] T. Ma, J. Pandit, S.V. Ekkad, S.T. Huxtable, Q.W. Wang, Simulation of thermoelectric-hydraulic performance of a thermoelectric power generator with longitudinal vortex generators, Energy 84 (2015) 695–703.
[32] S. Deshpande, B.V. Ravi, J. Pandit, T. Ma, S. Huxtable, S. Ekkad, Effect of longitudinal vortex generator location on thermoelectric-hydraulic performance of a single stage integrated thermoelectric power generator, in: Proceedings of the ASME 2015 International Mechanical Engineering Congress and Exposition, 2015, IMECE2015-52244.
[33] C. Liu, J.T. Teng, J.C. Chu, Y.L. Chiu, S.Y. Huang, S.P. Jin, T. Dang, R. Greif, H.H. Pan, Experimental investigations on liquid flow and heat transfer in rectangular microchannel with longitudinal vortex generators, Int. J. Heat Mass Transfer 54 (2011) 3069–3080.
[34] C. Chen, J.T. Teng, C.H. Cheng, S.P. Jin, S.Y. Huang, C. Liu, M.T. Lee, H.H. Pan, R. Greif, A study on fluid flow and heat transfer in rectangular microchannels with various longitudinal vortex generators, Int. J. Heat Mass Transfer 69 (2014) 203–214.
[35] A. Ebrahimi, E. Roohi, S. Kheradmand, Numerical study of liquid flow and heat transfer in rectangular microchannel with longitudinal vortex generators, Appl. Thermal Eng. 78 (2015) 576–583.
[36] A. Ebrahimi, F. Rikhtegar, A. Sabaghan, E. Roohi, Heat transfer and entropy generation in a microchannel with longitudinal vortex generators using nanofluids, Energy 101 (2016) 190–201.
[37] A. Sabaghan, M. Edalatpour, M.C. Moghadam, E. Roohi, H. Niazmand, Nanofluid flow and heat transfer in a microchannel with longitudinal vortex generators: Two-phase numerical simulation, Appl. Thermal Eng. 100 (2016) 179–189.
[38] X.J. Wei, Y.K. Joshi, P.M. Ligrani, Numerical simulation of laminar flow and heat transfer inside a micro-channel with one dimpled surface, ASME Trans. J. Electron. Packag. 129 (1) (2007) 63–70.
[39] FLUENT 15.0 user's guide, FLUENT Inc., 2013.
[40] D.L. Gee, R.L. Webb, Forced convection heat transfer in helically rib-roughened tubes, Int. J. Heat Mass Transfer 23 (8) (1980) 1127–1136.
[41] M. Khoshvaght-Aliabadi, O. Sartipzadeh, A. Alizadeh, An experimental study on vortex-generator insert with different arrangements of delta-winglets, Energy 82 (2015) 629–639.